

## Thermal conductivity of nanoparticle suspensions

Shawn A. Putnam,<sup>a)</sup> David G. Cahill, and Paul V. Braun

*Department of Materials Science and Engineering, Frederick Seitz Materials Research Laboratory, University of Illinois, Urbana, Illinois 61801 and Center for Advanced Materials for Purification of Water with Systems, University of Illinois, Urbana, Illinois 61801*

Zhenbin Ge and Robert G. Shimmin

*Department of Materials Science and Engineering, Frederick Seitz Materials Research Laboratory, University of Illinois, Urbana, Illinois 61801*

(Received 21 July 2005; accepted 24 February 2006; published online 26 April 2006)

We describe an optical beam deflection technique for measurements of the thermal diffusivity of fluid mixtures and suspensions of nanoparticles with a precision of better than 1%. Our approach is tested using the thermal conductivity of ethanol-water mixtures; in nearly pure ethanol, the increase in thermal conductivity with water concentration is a factor of 2 larger than predicted by effective medium theory. Solutions of C<sub>60</sub>-C<sub>70</sub> fullerenes in toluene and suspensions of alkanethiolate-protected Au nanoparticles were measured to maximum volume fractions of 0.6% and 0.35 vol %, respectively. We do not observe anomalous enhancements of the thermal conductivity that have been reported in previous studies of nanofluids; the largest increase in thermal conductivity we have observed is 1.3% ± 0.8% for 4 nm diam Au particles suspended in ethanol. © 2006 American Institute of Physics. [DOI: 10.1063/1.2189933]

### I. INTRODUCTION

Nanofluids are fluid suspensions of solid nanoparticles or nanofibers with particle sizes <100 nm. These fluid composites have attracted much attention since anomalously large enhancements in thermal conductivities were reported in 2001.<sup>1,2</sup> In addition to enhanced thermal conductivities, other desirable heat transfer properties have also been reported: for example, nanofluids with temperature-dependent thermal conductivities,<sup>3</sup> increased critical heat fluxes in boiling heat transfer,<sup>4-7</sup> and increased heat transfer in forced convection.<sup>8,9</sup>

A vast majority of the experimental work on the thermal properties of nanofluids has focused on the thermal conductivity.<sup>1,3,10-22</sup> Typically, thermal conductivities of nanofluids are measured with the transient hot-wire method.<sup>1,12-20</sup> Parallel plate geometries have been used less frequently.<sup>3,10,11</sup>

Large enhancements in the thermal conductivity of nanofluids containing spherical particles, or strong temperature dependence of the thermal conductivity, cannot be explained by effective medium theory. As a result, within the last few years, several theoretical models have been proposed.<sup>10,23-31</sup> Some of these models have focused on the Brownian motion of nanoparticles as a basis for explaining the anomalous thermal conductivities.<sup>10,23,24</sup> Others have noted, however, that the time scales for Brownian motion of the particles are far too slow to explain such a large enhancement in thermal conductivity.<sup>32</sup> Unfortunately, the investigations of the properties of nanofluids have reached the awkward situation of having a greater number of competing theoretical models than systematic experimental results.

To help address this situation, we have studied the ther-

mal conductivity of well-characterized and stable suspensions of fullerene molecules and alkanethiolate-protected Au nanoparticles. Our experimental technique is accurate, precise, and relatively immune to errors created by radiative heat transfer or heat transfer by convection.

### II. EXPERIMENTAL DETAILS

#### A. Materials and preparation of nanofluid suspensions

The nanofluids used in this work consisted of mixtures of C<sub>60</sub>-C<sub>70</sub> fullerene in toluene and alkanethiolate-stabilized Au nanoparticles in ethanol and toluene. Additional experiments were conducted with water/ethanol mixtures and dyes of indigo carmine in deionized water. The Au nanoparticles in ethanol were functionalized with 11-mercapto-1-undecanol (MUD) and have a Au core diameter of  $d \approx 4$  nm. The Au nanoparticles in toluene were functionalized with dodecanethiol and have a Au core diameter of  $d \approx 2$  nm. The diameters of the Au nanoparticles were measured by transmission electron microscopy (TEM). All of our Au-based nanofluids were prepared in wt % by first drying the synthesized nanofluids to a waxy solid and then diluting with ethanol or toluene on a digital balance. In this work, we refer to the Au nanoparticles in ethanol and toluene as Au-MUD and Au-C<sub>12</sub>, respectively.

The 4 nm Au-MUD nanoparticles in ethanol were made using a one-phase synthesis. The synthesis procedure is similar to that described in Ref. 33. Under vigorous stirring at room temperature, 2 mmol of MUD was added to a 2 mmol solution of hydrogen tetrachloroaurate (HAuCl<sub>4</sub>) in 10 ml of anhydrous tetrahydrofuran (THF). After stirring for  $\approx 20$  min, a 1M solution of lithium triethylborohydride in THF was then added dropwise until the evolution of gas could no longer be observed. The particles were cleaned by

<sup>a)</sup>Electronic mail: sputnam@uiuc.edu

first centrifuging in THF (three times—discarding the supernatant) and then dialyzing in ethanol. After cleaning, the suspension was allowed to aggregate for several weeks and then the sediment was discarded.

The 2 nm Au-C<sub>12</sub> nanoparticles in toluene were made using a two-phase synthesis. Our synthesis procedure followed Ref. 34; the ratio of dodecanethiol to Au was 3:1.

The concentrations of our nanoparticle suspensions were determined most directly in wt %; conversion to vol % requires consideration of the mass density of the particles. For a dilute suspension, the conversion from wt %  $f_p$  to vol %  $\phi_p$  is simply  $\phi_p \approx (\rho_f/\rho_p)f_p$ , where  $\rho_f$  is the density of the base fluid and  $\rho_p$  is the density of the nanoparticles.

We assume a density of  $\rho_p \approx 1.7 \text{ g cm}^{-3}$  for the C<sub>60</sub>-C<sub>70</sub> fullerenes and use  $\rho_f = 0.867 \text{ g cm}^{-3}$  for the density of toluene. The alkanethiolate-protected Au nanoparticles are, however, core-shell particles, so  $\rho_p$  was calculated based upon the diameter of the Au core  $d_{\text{Au}}$ , the thickness of the alkanethiolate shell  $l$ , and the mass ratio of the shell to the Au core  $x = m_{\text{shell}}/m_{\text{Au}}$ . We estimate  $\rho_p \approx 5.39 \text{ g cm}^{-3}$  for the Au-MUD particles, where  $d_{\text{Au}} = 4 \text{ nm}$ ,  $l = 1.2 \text{ nm}$ , and  $x = 1/7$ . Similarly,  $\rho_p \approx 2.42 \text{ g cm}^{-3}$  for the Au-C<sub>12</sub> particles, where  $d_{\text{Au}} = 2 \text{ nm}$ ,  $l = 1.2 \text{ nm}$ , and  $x = 1/3$ . The shell thicknesses and shell/core mass ratios are from Refs. 35 and 36. The volume fraction of the Au core was then estimated as  $\phi_{\text{Au}} = g\phi_p$ , where  $g$  is the ratio of the Au core volume to the total particle volume.

## B. Measurement technique and raw data

To measure the thermal conductivity, we used a micron-scale beam deflection technique we developed for measurements of the Soret coefficient of fluids.<sup>37</sup> The approach is based upon the deflection of a laser beam created by a gradient in the index of refraction in the fluid. The index of refraction gradient is created by alternately heating a pair of parallel Au thin-film lines fabricated by photolithography on a fused silica (FS) substrate. The Au line heaters are in direct contact with both the fluid and the FS substrate in a sealed fluid cell possessing a cylindrical geometry (see Sec. II in Ref. 37). The line heaters are separated by 50  $\mu\text{m}$  and have a width of 6  $\mu\text{m}$ . We mount the fluid cell on a two axis tilt stage and heat from above. The laser beam first passes between the metal line heaters on the FS substrate and then through the fluid under study. The periodic beam deflections existing the fluid cell are measured with a position-sensitive detector and lock-in amplifier. Following each experiment the fluid cell is dismantled, cleaned, and dried with nitrogen gas.

We note that the particles of unstable nanofluids flocculate and form agglomerates on the metal line heaters, exit window, and FS substrate; in result, the intensity of the laser beam existing the cell is decreased when passed through such clustered regions. To ensure that data for only uniform dispersions are reported, we monitor the intensity of the laser beam existing the cell and discard suspensions that show changes in stability and homogeneity.

Figure 1 shows an example of our raw data for the beam deflections as a function of modulation frequency with com-

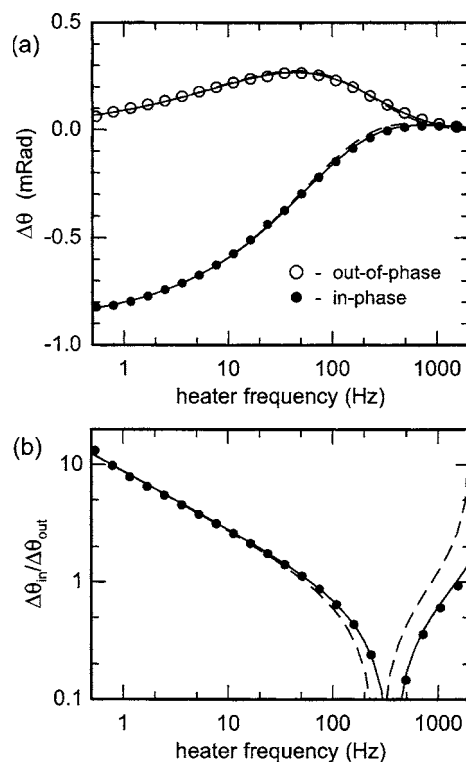


FIG. 1. Comparison between experimental data (symbols) and theoretical calculations (lines) for the deflection of the laser beam through a sample cell containing ethanol as a function of heater frequency. The amplitude of the temperature oscillations is  $\Delta T_{\text{osc}} \approx 2 \text{ K}$ . (a) The filled symbols are the in-phase (real) part of the beam deflection and open symbols are the out-of-phase (imaginary) part. (b) The ratio of the real and imaginary components of the beam deflection as a function of heater frequency. In both (a) and (b), the dashed line is for a laser beam radius of  $w_0 = 0$  and the solid line is for  $w_0 = 7.5 \mu\text{m}$ .

parisons to the analytical model for the beam deflection.<sup>37</sup> In Fig. 1, all model parameters are determined by independent measurements or are taken from literature; i.e., the heater dimensions, thermal properties, and optical properties of the FS heater substrate were verified independently,<sup>38</sup> and the heat capacity ( $C_p = 1.913 \text{ J cm}^{-3} \text{ K}^{-1}$ ), thermo-optic coefficient ( $dn/dT = 4.07 \times 10^{-4} \text{ K}^{-1}$ ), and thermal conductivity ( $\Lambda = 1.635 \text{ mW cm}^{-1} \text{ K}^{-1}$ ) of ethanol were taken from Refs. 39–41, respectively.

With respect to our previous studies,<sup>37,42</sup> one new parameter was added to our analytical model to correct for the finite size of the focal spot of the laser beam  $w_0$ . In short, a factor of  $\exp[-(kw_0/2)^2]$  was included in the integrand of Eq. (9) of Ref. 37 to create a Gaussian-weighted average of the beam deflection over a region of width  $w_0$ . Treating  $w_0$  as a fitting parameter gives  $w_0 = 7.5 \mu\text{m}$ , see Fig. 1. The diffraction-limited beam waist we calculate from the diameter of the laser beam and the focal lengths of the lenses is  $w_0 = 10.1 \mu\text{m}$  which is close to the value of  $w_0$  derived from the fit to the beam deflection data. For all subsequent data analysis, the parameter  $w_0$  was fixed at  $w_0 = 7.5 \mu\text{m}$ .

To determine the thermal conductivity, we analyze the phase of the beam deflection at heating frequency  $f = 33.09 \text{ Hz}$  chosen to maximize the sensitivity of our measurement to the thermal diffusivity of the fluid while minimizing systematic errors introduced by thermodiffusion at

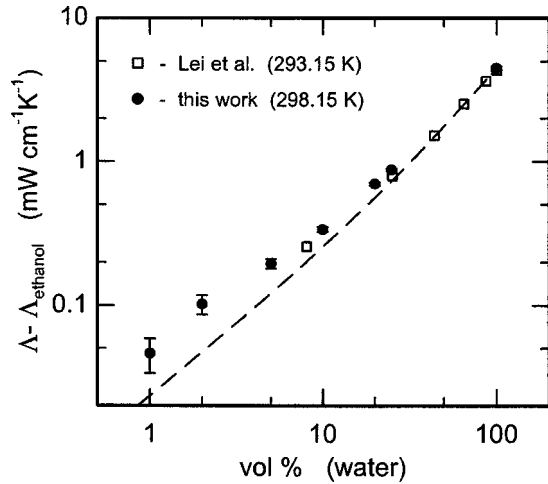


FIG. 2. Difference between the thermal conductivity of water/ethanol mixtures and thermal conductivity of pure ethanol. Data by Lei *et al.*, Ref. 41, are included for comparison. The dashed line is the prediction of the symmetric effective medium theory, see Refs. 49 and 50. The thermal conductivity of pure ethanol at  $\approx 25^\circ\text{C}$  is  $\Lambda_{\text{EtOH}} = 1.609 \pm 0.011 \text{ mW cm}^{-1} \text{ K}^{-1}$ .

lower frequency or the beam position at higher frequencies. Figure 1(b) is a plot of the ratio of the in-phase and out-of-phase components of the beam deflection as a function of heater frequency. In a typical experiment, the phase of the beam deflection at  $f = 33.09 \text{ Hz}$  is recorded once every few minutes and averaged over an  $\approx 20 \text{ min}$  interval.

### C. Water/ethanol mixtures

Experiments were conducted with water/ethanol mixtures to verify the accuracy and demonstrate the precision of our measurements, see Fig. 2. We measure  $\Lambda_{\text{EtOH}} = 1.609 \pm 0.011 \text{ mW cm}^{-1} \text{ K}^{-1}$  for pure ethanol at  $T \approx 25^\circ\text{C}$ , where Lei *et al.* report  $\Lambda_{\text{EtOH}} = 1.635 \text{ mW cm}^{-1} \text{ K}^{-1}$  at  $T \approx 20^\circ\text{C}$ . This difference is consistent with the fact that the thermal conductivity of ethanol decreases with increasing temperature.<sup>43</sup>

Interestingly, low concentrations of water have a much larger effect on the thermal conductivity of ethanol-rich mixtures than predicted by effective medium theory. For example, a 2 vol % concentration of water increases the thermal conductivity of ethanol by  $\approx 6\%$  while the prediction of the symmetric effective medium theory is an increase of only  $\approx 3\%$ , half of the measured value.

### D. Indigo-carmine dyes in water

Because our nanofluids of Au nanoparticles and  $\text{C}_{60}$ – $\text{C}_{70}$  fullerenes absorb light at the wavelength ( $\lambda = 633 \text{ nm}$ ) of the He–Ne laser used in the measurements, we conducted experiments with dyes of indigo carmine in aqueous solution to verify the accuracy of our measurements of optically absorbing fluids. Within the precision of our experiments, we did not observe changes in the thermal conductivity  $\Lambda$  of water containing indigo carmine. At  $25^\circ\text{C}$ ,  $\Lambda = 6.15 \pm 0.11$ , and  $6.08 \pm 0.06$  and  $6.19 \pm 0.06 \text{ mW cm}^{-1} \text{ K}^{-1}$ , for pure water and dye concentrations of  $f \approx 0.14 \text{ wt } \%$  and  $f \approx 0.03 \text{ wt } \%$ , respectively. At  $f \approx 0.14 \text{ wt } \%$ , the intensity of the laser exist-

ing the sample cell was reduced by  $\approx 80\%$ , twice the attenuation measured in our experiments with Au and fullerene nanofluids at their highest particle loadings.

### E. Effects of thermodiffusion

In liquid mixtures and particle suspensions, temperature gradients also produce gradients in the index of refraction due to mass transport driven by the temperature gradients, i.e., due to thermodiffusion or the Soret effect.<sup>42</sup>

As expected at low heating frequencies,  $f < D_c / (\pi a^2)$  Hz, we observe concentration gradients in the water/ethanol mixtures due to thermodiffusion, where  $D_c \approx 1 \times 10^{-5} \text{ cm}^2 \text{ s}^{-1}$  is the diffusion coefficient of water in ethanol,  $2a \approx 50 \mu\text{m}$  is the line-heater separation, and  $1/f$  is the time required for water to diffuse half the distance between the metal heaters. This corresponds to low frequencies  $f < 0.5 \text{ Hz}$  and, therefore, the influence on our analysis of the beam deflection data at  $f = 33.09 \text{ Hz}$  is small and less than the other systematic errors in our experiment. Nevertheless, we accounted for thermodiffusion in our analysis of  $\Lambda$  for water/ethanol mixtures using  $dn/dT$ ,  $cdn/dc$ ,  $D_c$ , and thermodiffusion coefficients published previously.<sup>40</sup> Our independent measurements of the thermodiffusion and diffusion constants of a 5 vol % water/ethanol mixture are within 15% of the prior results.<sup>40</sup>

We did not observe the effects of thermodiffusion in our suspensions of  $\text{C}_{60}$ – $\text{C}_{70}$  fullerenes or alkanethiolate-protected Au nanoparticles. This is reasonable considering that our nanofluids are relatively dilute and the sensitivity of our experiments to thermodiffusion scales with the product of the particle concentration, the Soret coefficient, and the change in the index of refraction with particle concentration.<sup>37</sup> We estimate an upper bound on the magnitude of the Soret coefficient at  $|S_T| < 0.01 \text{ K}^{-1}$  for the fullerene suspensions and  $|S_T| < 0.1 \text{ K}^{-1}$  for the Au-based nanofluids.

### F. Effects of radiative and convective heat transfer

Our technique is relatively immune to errors created by radiation and convection. As stated in Sec. II B, our micron-scale beam deflection apparatus was developed to measure the Soret coefficients of liquid mixtures and nanoparticle suspensions. Therefore, our ability to reliably produce steady-state concentration gradients in our previous work supports the absence of convective flows.<sup>37,42</sup> In regard to radiation, the small geometry of our line heaters supports that even with measurements at unrealistic temperatures of 1000 K the errors due to radiative heat losses by the metal heaters are less than 0.3%, see Sec. II in Ref. 44.

### G. Characterization of Au suspensions by UV-vis spectroscopy

UV-vis spectroscopy was used to measure the absorption spectra in the vicinity of the surface plasmon absorbance, see Fig. 3. For monodisperse core-shell metal nanoparticles with radii much less than the wavelength of the incoming light,  $r \ll \lambda$ , the absorption coefficient of the suspension can be approximated as

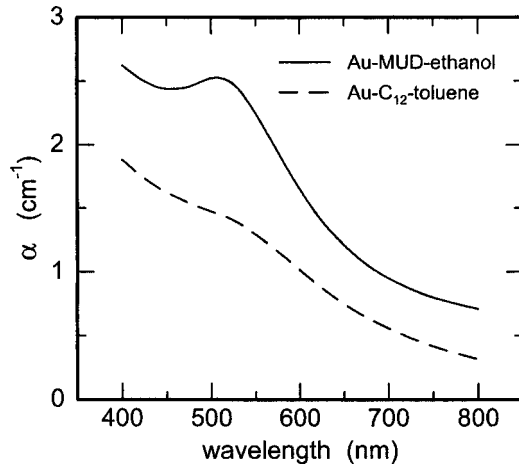


FIG. 3. UV-vis absorption spectra for alkanethiol-functionalized Au nanoparticles. The Au-MUD nanoparticles in ethanol have a Au core diameter of 4 nm and were measured at a particle concentration of  $\phi_{\text{Au}} \approx 0.39 \times 10^{-3}$  vol %. The Au-C<sub>12</sub> nanoparticles in toluene have a Au core diameter of 2 nm and were measured at a particle concentration of  $\phi_{\text{Au}} \approx 0.135 \times 10^{-3}$  vol %.

$$\alpha \approx \left( \frac{6\pi n \phi_{\text{Au}}}{\lambda g} \right) \times \text{Im} \left[ \frac{(\epsilon_s - n^2)(\epsilon_{\text{Au}} - 2\epsilon_s) + g(\epsilon_{\text{Au}} - \epsilon_s)(n^2 + 2\epsilon_s)}{(\epsilon_s + 2n^2)(\epsilon_{\text{Au}} + 2\epsilon_s) + g(2\epsilon_s - 2n^2)(\epsilon_{\text{Au}} - \epsilon_s)} \right], \quad (1)$$

where  $n$  is the index of refraction of the fluid,  $\phi_{\text{Au}}$  is the volume fraction of Au,  $g$  is the ratio of the Au core volume to the total core-shell particle volume,  $\epsilon_{\text{Au}}$  is the complex dielectric function of bulk Au,  $\epsilon_s$  is the dielectric function of the alkanethiolate shell, and  $\text{Im}$  represents the imaginary part of the complex expression within the brackets.<sup>45</sup> For  $g=1$  the shell thickness is zero and Eq. (1) reduces to the form of an uncoated sphere [see Eq. (5) in Ref. 45]. As mentioned in Sec. II A, we assume an alkanethiolate shell thickness of 1.2 nm; therefore,  $g \approx 0.244$  for the 4 nm Au-MUD nanoparticles in ethanol and  $g \approx 0.094$  for the 2 nm Au-C<sub>12</sub> nanoparticles in toluene.

To check the concentration of Au in our nanofluids, we compare our measured UV-vis data with the predictions of Eq. (1) at  $\lambda=440$  nm. We evaluate Eq. (1) using the dielectric data of bulk Au from Ref. 46 ( $\epsilon_{\text{Au}} = -1.725 + i5.47$  at  $\lambda=440$  nm) and the dielectric constant of dodecanethiol for the shell [ $\epsilon_s \approx (1.46)^2$ , see Ref. 47]. Our choice of analysis at  $\lambda=440$  nm is because the influence of particle size on the absorption spectra is minimized at wavelengths below the surface plasmon absorption band, see, for example, Fig. 2 of Ref. 48. The measured optical absorption is in good agreement with these predictions and gives us confidence in the characterization of the nanoparticles. We measure  $\alpha \approx 2.45$  cm<sup>-1</sup> with the 4 nm Au-MUD-ethanol nanofluids at a particle concentration of  $\phi_{\text{Au}} \approx 0.39 \times 10^{-3}$  vol %, where Eq. (1) predicts  $\alpha \approx 2.75$  cm<sup>-1</sup>. Similarly, for the 2 nm Au-C<sub>12</sub>-toluene nanofluids ( $\phi_{\text{Au}} \approx 0.135 \times 10^{-3}$  vol %), we measure  $\alpha \approx 1.66$  cm<sup>-1</sup> and calculate  $\alpha \approx 1.74$  cm<sup>-1</sup>.

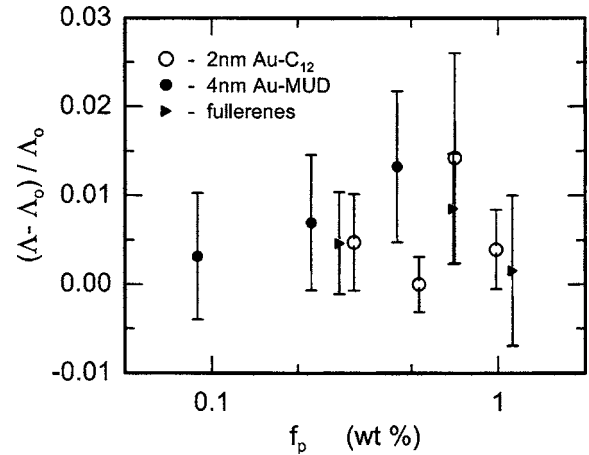


FIG. 4. Relative changes in the thermal conductivity of nanofluids at room temperature as a function of nanoparticle concentration in wt %  $f_p$ . Open circles (2 nm Au-C<sub>12</sub>) are data for the dodecanethiol-functionalized Au nanoparticles in toluene, filled circles (4 nm Au-MUD) are data for the MUD-functionalized Au nanoparticles in ethanol, and filled triangles are data for C<sub>60</sub>-C<sub>70</sub> fullerenes in toluene.

### III. RESULTS FOR NANOFLUIDS

Figure 4 shows our data for the relative changes in the thermal conductivity of nanofluids as a function of nanoparticle loading in wt %  $f_p$ . For each nanofluid, the thermal conductivity of the base fluid ( $\Lambda_0$ ) was measured independently at the same temperature as the nanofluid; the measurement temperature is approximately constant for each set of data, but because our sample cell is not temperature controlled, the temperatures of measurements for each set of samples vary with the temperature of our laboratory between 25 and 28 °C.

The same data are replotted in Figs. 5 and 6 with a change in the scaling of the  $x$  axis; in Fig. 5, the  $x$  axis is the volume fraction of the nanoparticle core  $\phi_{\text{core}}$  and in Fig. 6, the  $x$  axis is the combined volume fraction of the nanoparticle core and the nanoparticle shell  $\phi_p$ . (For the fullerenes in toluene  $\phi_p \approx \phi_{\text{core}} \approx 0.51 f_p$ , for the 2 nm Au-C<sub>12</sub> nanopar-

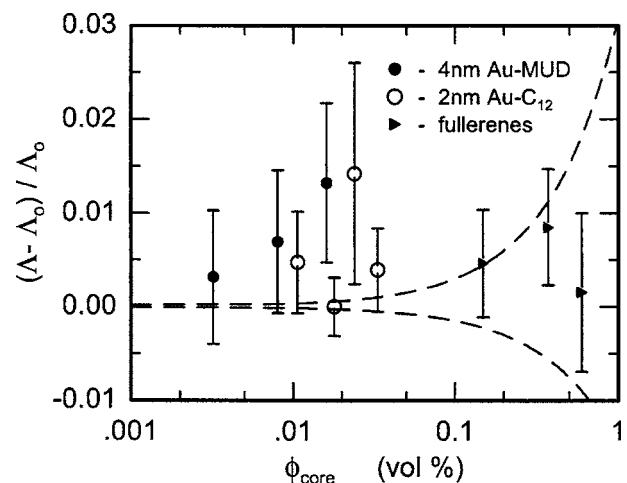


FIG. 5. Relative changes in the thermal conductivity of nanofluids as a function of the volume fraction of the nanoparticle core. The dashed lines are the predictions of effective medium theory for nanofluids containing highly thermally conductive nanoparticles (upper) and thermally insulating nanoparticles (lower).

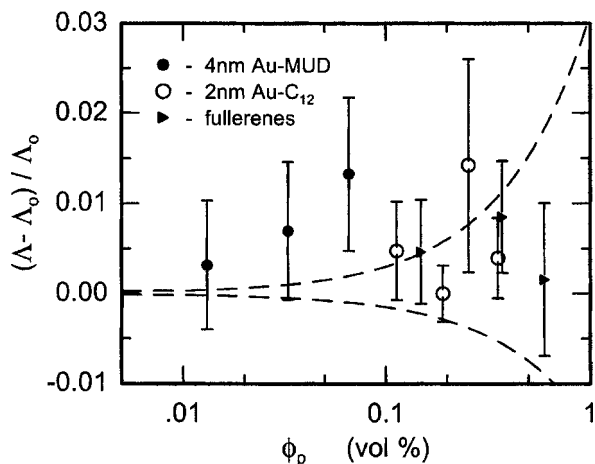


FIG. 6. Relative changes in the thermal conductivity of nanofluids as a function of the volume fraction of the entire particle. (For fullerene molecules, the volume fraction of the core and the volume fraction of the entire particle are the same.) In the conversion to  $\phi_p$  from the measured particle concentrations in wt % ( $f_p$ ), an alkanethiol shell thickness of  $l \approx 1.2$  nm was used for both the 2 nm Au-C<sub>12</sub> nanoparticles in toluene and the 4 nm Au-MUD nanoparticles in ethanol (see Sec. II A). The dashed lines are the predictions of effective medium theory for nanofluids containing highly thermally conductive nanoparticles (upper) and thermally insulating nanoparticles (lower).

ticles in toluene  $\phi_p \approx 10.64\phi_{\text{Au}} \approx 0.358f_p$ , and for the 4 nm Au-MUD nanoparticles in ethanol  $\phi_p \approx 4.1\phi_{\text{Au}} \approx 0.147f_p$ .) The data are also compared to the upper and lower limits of the predictions of effective medium theory<sup>49,50</sup> for spherical particles. With the exception of the Au-MUD and Au-C<sub>12</sub> data at  $\phi_{\text{core}} \approx 0.02$  vol %, all measurements are consistent with a thermal conductivity that is independent of particle loading, in agreement with the predictions of effective medium theory at low values of the particle loading.

#### IV. CONCLUSIONS

We do not observe a significant enhancement in the thermal conductivity of fluids that are loaded by small volume fractions of nanoparticles. Within the context of effective medium theory, these findings are expected: effective medium theory predicts that the largest possible increase in the thermal conductivity of a fluid loaded by a volume fraction  $\phi \ll 1$  of spherical particles will be  $3\phi\Lambda_0$ . Our experimental results are, however, in direct conflict with the anomalous results of Ref. 15 and recent theoretical models<sup>10,23</sup> that attempt to explain the anomalous experimental results.<sup>1,15</sup> Since we have not been able to synthesize and study well-dispersed nanoparticle suspensions with concentrations greater than reported here, we cannot exclude the possibility that higher loadings of nanoparticles  $\phi > 0.01$  (1 vol %) could enhance the thermal conductivity of fluids to an extent significantly larger than the prediction of effective medium theory.

#### ACKNOWLEDGMENTS

This work is based upon work supported by the U.S. Department of Energy Grant No. DEFG02-01ER45938 and

the STC Program of the National Science Foundation under Agreement No. CTS-0120978. One of the authors (R.G.S.) acknowledges support from the Fannie & John Hertz Foundation.

- <sup>1</sup>J. A. Eastman, S. U. S. Choi, S. Li, W. Yu, and L. J. Thompson, *Appl. Phys. Lett.* **78**, 718 (2001).
- <sup>2</sup>P. Keblinski, J. A. Eastman, and D. G. Cahill, *Mater. Today* **8**, 36 (2005).
- <sup>3</sup>S. K. Das, N. Putra, P. Thiesen, and W. Roetzel, *ASME J. Heat Transfer* **125**, 567 (2003).
- <sup>4</sup>I. C. Bang and S. H. Chang, *Int. J. Heat Mass Transfer* **48**, 2407 (2005).
- <sup>5</sup>S. M. You and J. H. Kim, *Appl. Phys. Lett.* **83**, 3374 (2003).
- <sup>6</sup>S. K. Das, N. Putra, and W. Roetzel, *Int. J. Heat Mass Transfer* **46**, 851 (2003).
- <sup>7</sup>P. Vassallo, R. Kumar, and S. D'Amico, *Int. J. Heat Mass Transfer* **47**, 407 (2004).
- <sup>8</sup>Y. Xuan and Q. Li, *ASME J. Heat Transfer* **125**, 151 (2003).
- <sup>9</sup>D. Wen and Y. Ding, *Int. J. Heat Mass Transfer* **47**, 5181 (2004).
- <sup>10</sup>D. H. Kumar, H. E. Patel, V. R. R. Kumar, T. Sundararajan, T. Pradeep, and S. K. Das, *Phys. Rev. Lett.* **93**, 144301 (2004).
- <sup>11</sup>X. Wang, X. Xu, and S. J. S. Choi, *J. Thermophys. Heat Transfer* **13**, 474 (1999).
- <sup>12</sup>S. U. S. Choi, Z. G. Zhang, W. Yu, F. E. Lockwood, and E. A. Grulke, *Appl. Phys. Lett.* **79**, 2252 (2001).
- <sup>13</sup>H. Xie, H. Lee, W. Youn, and M. Choi, *J. Appl. Phys.* **94**, 4967 (2003).
- <sup>14</sup>D. Wen and Y. Ding, *J. Thermophys. Heat Transfer* **18**, 481 (2004).
- <sup>15</sup>H. E. Patel, S. K. Das, T. Sundararajan, A. S. Nair, B. George, and T. Pradeep, *Appl. Phys. Lett.* **83**, 2931 (2003).
- <sup>16</sup>T.-K. Hong, H.-S. Yang, and C. Choi, *J. Appl. Phys.* **97**, 064311 (2005).
- <sup>17</sup>H. Xie, J. Wang, T. Xi, Y. Liu, F. Ai, and Q. Wu, *J. Appl. Phys.* **91**, 4568 (2002).
- <sup>18</sup>H. Xie, J. Wang, T. Xi, Y. Liu, and F. Ai, *J. Mater. Sci. Lett.* **21**, 1469 (2002).
- <sup>19</sup>H. Xie, J. Wang, J. Xi, and Y. Liu, *Int. J. Thermophys.* **23**, 571 (2002).
- <sup>20</sup>Y. Xuan and Q. Li, *Int. J. Heat Fluid Flow* **21**, 58 (2000).
- <sup>21</sup>H. Masuda, A. Ebata, K. Teramae, and N. Hishinuma, *Netsu Bussei* **7**, 227 (1993).
- <sup>22</sup>M. J. Biercuk, M. C. Liaguno, M. Radosavljevic, J. K. Hyun, A. T. Johnson, and J. E. Fischer, *Appl. Phys. Lett.* **80**, 2767 (2004).
- <sup>23</sup>R. Prasher, R. Bhattacharya, and R. E. Phelan, *Phys. Rev. Lett.* **94**, 025901 (2005).
- <sup>24</sup>S. P. Jang and S. U. S. Choi, *Appl. Phys. Lett.* **84**, 4316 (2004).
- <sup>25</sup>K. Khanafer, K. Vafai, and M. Lightstone, *Int. J. Heat Mass Transfer* **46**, 3639 (2003).
- <sup>26</sup>H. Xie, M. Fujii, and X. Zhang, *Int. J. Heat Mass Transfer* **48**, 2926 (2005).
- <sup>27</sup>Q. Xue, *Phys. Lett. A* **307**, 313 (2003).
- <sup>28</sup>Q. Xue and W. Xu, *Mater. Chem. Phys.* **90**, 298 (2005).
- <sup>29</sup>L. Gosselin and A. K. da Silva, *Appl. Phys. Lett.* **85**, 4160 (2004).
- <sup>30</sup>A. R. A. Khaled and K. Vafai, *Int. J. Heat Mass Transfer* **48**, 2172 (2005).
- <sup>31</sup>Y. Xuan and W. Roetzel, *Int. J. Heat Mass Transfer* **43**, 3701 (2000).
- <sup>32</sup>P. Keblinski, S. R. Phillpot, S. U. S. Choi, and J. A. Eastman, *Int. J. Heat Mass Transfer* **45**, 855 (2002).
- <sup>33</sup>C. K. Yee, R. Jordan, A. Ulman, H. White, A. King, M. Rafailovich, and J. Sokolov, *Langmuir* **15**, 3486 (1999).
- <sup>34</sup>M. Brust, M. Walker, D. Bethell, D. J. Schiffrin, and R. Whyman, *J. Chem. Soc., Chem. Commun.* **1994**, 801.
- <sup>35</sup>R. G. Terrill, *J. Am. Chem. Soc.* **117**, 12537 (1995).
- <sup>36</sup>M. J. Hostetler *et al.*, *Langmuir* **14**, 17 (1998).
- <sup>37</sup>S. A. Putnam and D. G. Cahill, *Rev. Sci. Instrum.* **75**, 2368 (2004).
- <sup>38</sup>The thermal conductivity ( $\Lambda \approx 13.4$  mW cm<sup>-1</sup> K<sup>-1</sup>), thermo-optic coefficient ( $dn/dT \approx 8.5 \times 10^{-6}$  K<sup>-1</sup>), and effective beam waist of the laser ( $\omega_0 \approx 7.5$   $\mu$ m) were determined in independent experiments with the fused silica (FS) heater substrate in air. In this analysis, we used a heat capacity of  $C_p \approx 1.64$  J cm<sup>-3</sup> K<sup>-1</sup>. The metal-line heater dimensions (separation— $2a = 50$   $\mu$ m and width— $2b = 6$   $\mu$ m) were verified with an optical microscope.
- <sup>39</sup>G. C. Benson and P. J. D'Arcy, *J. Chem. Eng. Data* **27**, 439 (1982).
- <sup>40</sup>R. Kita, S. Wiegand, and J. Luettmer-Strathamann, *J. Chem. Phys.* **121**, 3874 (2004).
- <sup>41</sup>Q. F. Lei, R. S. Lin, and D. Y. Ni, *J. Chem. Eng. Data* **42**, 971 (1997).
- <sup>42</sup>S. A. Putnam and D. G. Cahill, *Langmuir* **21**, 5317 (2005).
- <sup>43</sup>D. N. Nikogosyan, *Properties of Optical and Laser-Related Materials: A*

*Handbook* (Wiley, Chichester, 1997).

<sup>44</sup>D. G. Cahill, *Rev. Sci. Instrum.* **61**, 802 (1990).

<sup>45</sup>P. Mulvaney, *Langmuir* **12**, 788 (1996).

<sup>46</sup>P. B. Johnson and R. W. Christy, *Phys. Rev. B* **6**, 4370 (1972).

<sup>47</sup>S. K. Ghosh, S. Nath, S. Kundu, K. Esumi, and T. Pal, *J. Phys. Chem. B*

**108**, 13963 (2004).

<sup>48</sup>L. B. Scaffardi, N. Pellegrini, L. de Sanctis, and J. L. Tocho, *Nanotechnology* **16**, 158 (2005).

<sup>49</sup>D. A. G. Bruggeman, *Ann. Phys.* **24**, 636 (1935).

<sup>50</sup>R. Landauer, *Inst. Phys. Conf. Ser.* **40**, 15 (1978).